

PHYSICAL SCIENCES

Dynamical interplay between superconductivity and pseudogap in cuprates as revealed by terahertz third-harmonic generation spectroscopy

Jiayu Yuan¹, Liyu Shi¹, Li Yue¹, Bohan Li², Zixiao Wang¹, Shuxiang Xu¹, Tiequan Xu³, Yue Wang^{3,4}, Zizhao Gan^{3,4}, Fucong Chen⁵, Zefeng Lin⁵, Xu Wang⁵, Kui Jin⁵, Xinbo Wang⁵, Jianlin Luo⁵, Sijie Zhang¹, Qiong Wu¹, Qiaomei Liu¹, Tianchen Hu¹, Rongsheng Li¹, Xinyu Zhou¹, Dong Wu², Tao Dong^{1*}, Nanlin Wang^{1,2,6*}

We report on nonlinear terahertz third-harmonic generation (THG) measurements on $\text{YBa}_2\text{Cu}_3\text{O}_{6+x}$ thin films. Different from conventional superconductors, the THG signal starts to appear in the normal state, which is consistent with the crossover temperature T^* of pseudogap over broad doping levels. Upon lowering the temperature, the THG signal shows an anomaly just below T_c in the optimally doped sample. Notably, we observe a beat pattern directly in the measured real-time waveform of the THG signal. We elaborate that the Higgs mode, which develops below T_c , couples to the mode already developed below T^* , resulting in an energy level splitting. However, this coupling effect is not evident in underdoped samples. We explore different potential explanations for the observed phenomena. Our research offers valuable insight into the interplay between superconductivity and pseudogap.

INTRODUCTION

The search for the underlying mechanism of superconductivity and its interplay with pseudogap state is at the heart of cuprate superconductors (1). A long-time controversial issue in the quest to understand the superconductivity in cuprates is whether the pseudogap state is a precursor to macroscopic coherent superconductivity or a distinct phase characterized by broken symmetries below the onset temperature T^* . Typical linear spectroscopic techniques or measurements under an equilibrium state for a superconductor are only sensitive to the single-particle excitation, enabling the determination of energy gaps developed in superconducting or pseudogap phases and characterization of different physical properties (2). By contrast, the collective excitations of superconductors cannot be accessed by these measurements, except for some special cases (3, 4). The superconductivity breaks global $U(1)$ gauge symmetry, and the associated collective modes are well understood. While the Nambu-Goldstone mode is shifted to plasma energy by the Anderson-Higgs mechanism, the Higgs mode locates at the energy corresponding to the minimum of the single-particle excitation spectrum with the energy of 2Δ at the long wavelength limit (5–8). The generation of sufficiently strong terahertz pulse (9) has enabled direct access to Higgs mode in superconductors via nonlinear optical coupling effect in the form of either free or forced oscillations in time domain (10, 11). When an intense narrow-band terahertz pulse is directed toward a superconductor, it can result in a third-harmonic

generation (THG) that exhibits a distinctive resonant enhancement at $2\omega = 2\Delta$ in the transmitted pulse. This phenomenon has been observed in various superconductors such as $\text{Nb}_{1-x}\text{Ti}_x\text{N}$, multiband MgB_2 , and d-wave cuprate superconductors (11–18), and is believed to be caused by the nonlinear interaction between the Higgs mode and terahertz wave. However, recent studies have suggested that, in addition to the Higgs mode, the Cooper pair breaking could also lead to the generation of THG with a similar resonant nature at $2\omega = 2\Delta$ (19). Their relative weight, and the visibility of the Higgs mode itself, strongly depends on the specific details of the system, such as the band structure, doping and disorder level (20, 21). Anyhow, the successful observation of superconductivity contributed terahertz THG signal in conventional superconductors has raised the hope for study of the interaction between different orders in dynamical fashion via coherent terahertz nonlinearities.

Cuprate superconductor is an ideal playground for exploring the dynamical interaction between Higgs mode and other distinct collective excitations (22–24). As cuprate systems have very complex phase diagrams, the interaction between superconductivity and other intertwined orders may modify the spectroscopic feature of the Higgs oscillation. The reported studies of Higgs mode by terahertz nonlinear Kerr (25, 26) and terahertz THG spectroscopy (27) in cuprates have generally focused on issue of which channel (Higgs mode (28) or Cooper pair breaking (19)) dominates the nonlinear THG and its temperature evolution. The interaction between Higgs mode and other distinct collective mode induced antiresonance in temperature dependence of THG intensity has been reported (27, 29, 30). However, the intertwined order coupling effect on Higgs oscillation waveform in cuprate superconductors remains largely unexplored.

Here, we report a systematic nonlinear terahertz THG study on five different doping $\text{YBa}_2\text{Cu}_3\text{O}_{6+x}$ (YBCO) thin films driven by multicycle strong field terahertz pulse (see Materials and Methods for additional experimental details). We identify a characteristic temperature T_{THG} below which the third-order susceptibility $\chi^{(3)}$

Copyright © 2024 The Authors, some rights reserved; exclusive licensee American Association for the Advancement of Science. No claim to original U.S. Government Works. Distributed under a Creative Commons Attribution NonCommercial License 4.0 (CC BY-NC).

¹International Center for Quantum Materials, School of Physics, Peking University, Beijing 100871, China. ²Beijing Academy of Quantum Information Sciences, Beijing 100193, China. ³Applied Superconductivity Center and State Key Laboratory for Mesoscopic Physics, School of Physics, Peking University, Beijing 100871, China. ⁴Peking University Yangtze Delta Institute of Optoelectronics, Nantong, Jiangsu, China. ⁵Beijing National Laboratory for Condensed Matter Physics, Institute of Physics, Chinese Academy of Sciences, Beijing 100190, China. ⁶Collaborative Innovation Center of Quantum Matter, Beijing, China. *Corresponding author. Email: taodong@pku.edu.cn (T.D.); nlwang@pku.edu.cn (N.W.)

starts to grow, and find that T_{THG} follows the trend of pseudogap developing temperature T^* or fluctuated superconductivity within our measured doping range. Upon entering the superconducting state, $\chi^{(3)}$ increases sharply but exhibits an abnormal dip feature near T_c which is more clearly seen in optimally doped sample. Unexpectedly, we observe a beat pattern directly in the measured real-time waveform of the THG signal. Fourier transformation of the time-domain spectrum results in two separate modes below and above original THG frequency. The observation strongly indicates that a new mode, being identified as Higgs mode, appears at T_c and couples to the mode already developed below T^* . However, this coupling effect becomes imperceptible in underdoped samples. We also perform similar measurements on an electron-doped cuprate sample $\text{La}_{2-x}\text{Ce}_x\text{CuO}_4$ ($x \sim 0.10$) (LCCO) without pseudogap phase and confirm the absence of THG above its T_c . We examine different potential explanations for the observed phenomena. Our research offers valuable insight into the interplay between superconductivity and pseudogap.

RESULTS

We start with the temperature dependence of THG intensity for five different doping level samples $P = 0.077, 0.08, 0.10, 0.138,$ and 0.15 driven by 60 kV/cm 0.5-THz multi-cycle pulse (the data for $P = 0.077$ doping are shown in the Supplementary Materials). Figure 1 (A to D) displays the typical real-time waveforms of THG signal. After fast Fourier transformation (FFT), the residual fundamental pulse after the high-frequency band-pass filter (1.5 THz) and the THG signal can be well separated in the frequency domain. To evaluate the temperature dependence of the THG signal, the spectral weight from 1.25 to 1.75 THz is integrated. As shown in Fig. 1 (E to H), the integrated THG intensity decreases continuously with temperature increasing toward T_c , except for the optimally doped sample, which represents a resonant enhancement of THG signal at temperature slightly below T_c . We will discuss the nature of resonance later. Above T_c , the THG signal still survives up to high temperature, which is in contrast to the conventional superconductors (11, 14–16) and iron-based superconductors (31, 32).

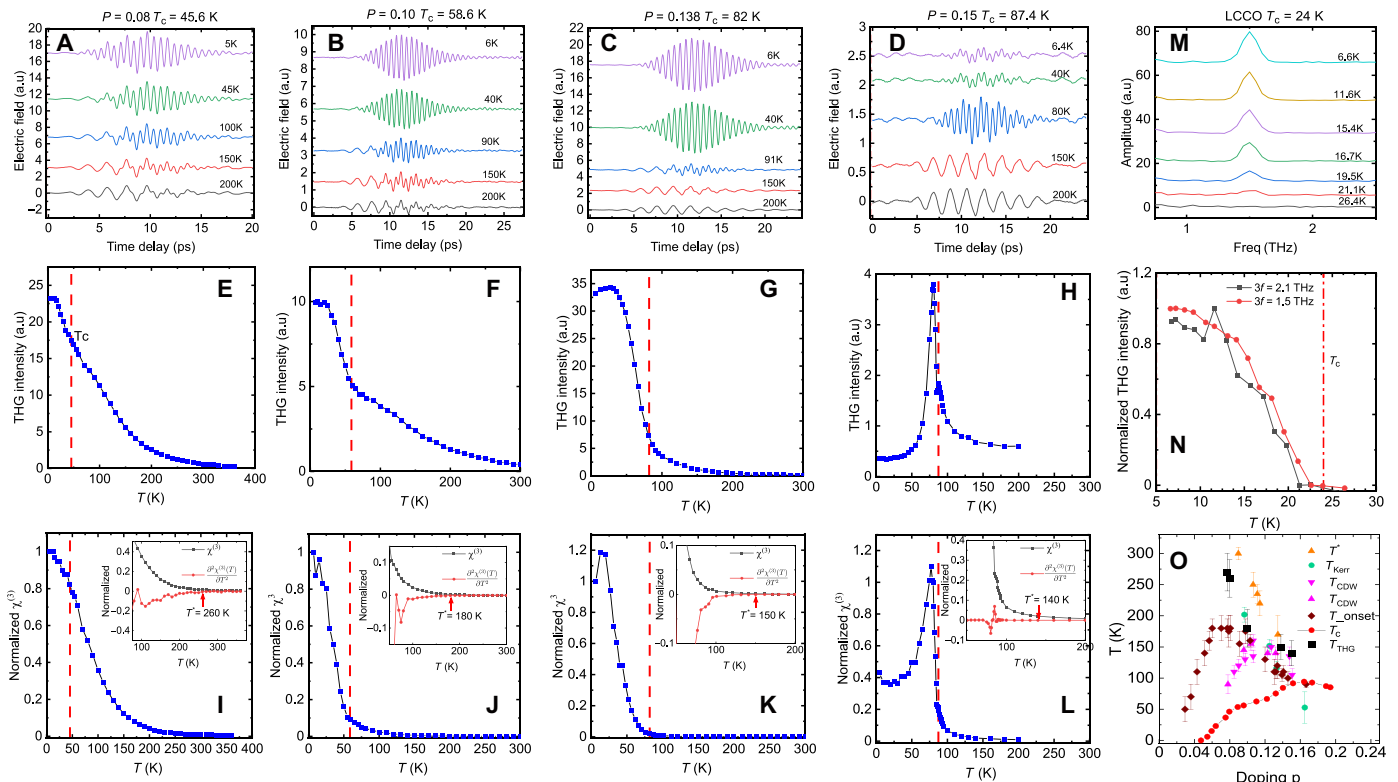


Fig. 1. Doping dependence of THG in YBCO and LCCO. (A to D) The real-time waveforms of the recorded THG signal after a high frequency ($3\omega = 1.5$ THz) band-pass filter at selected temperatures for (A) $P = 0.08$, (B) $P = 0.10$, (C) $P = 0.138$, (D) $P = 0.15$ YBCO thin films. (E to H) Temperature dependence of $I_{3\omega}$ from all four samples. The red dash lines label the T_c of the samples. (I to L) Temperature dependence of normalized third-order susceptibility $\chi^{(3)}(T)$ from all four samples. The insets show the second derivative of $\chi^{(3)}(T)$ with respect to temperature $\frac{\partial^2 \chi^{(3)}(T)}{\partial T^2}$. The red vertical arrows denote the crossing temperature of the rapid growing of the THG signals T_{THG} determined from the second derivative. (M) The THG spectrum of optimal doped LCCO with $T_c = 24$ K driven by 0.5-THz pulse. (N) Temperature dependence of $I_{3\omega}$ for LCCO sample. The THG intensity disappears abruptly when the temperature is higher than T_c . (O) Temperature-doping phase diagram of YBCO. Black squares represent the crossing temperature T_{THG} determined by the present terahertz THG spectroscopy. For comparison, the pseudogap temperatures determined by other probes are also plotted. Orange triangles are T^* reported by polarized neutron scattering (54), which are consistent with the T^* determined by transport measurements. Magenta triangles represent the formation temperature of the short-range CDW, T_{CDW} , reported by resonant x-ray measurements (48, 49). Green dots are the temperature T_{Kerr} below which the time-reversal symmetry is broken, reported by the polar Kerr effect (55). Red dots are the superconductivity transition temperature T_c , reported by resistivity measurements (56). Brown rhombus are the superconducting fluctuation temperatures T_{onset}^* determined by the c -axis infrared spectroscopy measurements (42).

The temperature dependence of raw THG intensity should be affected by the effective electric field inside the thin film because the effective driving field inside the thin film $E_{\omega}(T)$ decreases below T_c due to the increase of the reflectivity. To quantitatively evaluate the temperature dependent behavior of the THG signal and get an innate response of THG efficiency, we calculated the third-order nonlinear susceptibility $\chi^{(3)}(T)$ for all of the doping samples driven by 0.5-THz pulse. The $\chi^{(3)}(T)$ is estimated by simultaneous measurement of the THG and the residual fundamental frequency passing through one band-pass filter of 3ω : $\chi^{(3)} = E_{3\omega} / E_{\omega}^3$. The comparison between the above approximation and the calculation from the Fabry-Perot formula further illustrates the rationality of the above analysis, as shown in the Supplementary Materials. Figure 1 (I to L) shows the normalized $\chi^{(3)}$ as a function of temperatures for $P = 0.08, 0.10, 0.138,$ and 0.15 , respectively. The resonant behavior is still visible for optimal doping after taking account of the screening effect, which is distinct from the reported measurements (27). We will discuss it later. For $P = 0.10, 0.138$ thin films, $\chi^{(3)}$ increases monotonically as the temperature decreases from 300 K and shows a clear enhancement around T_c . However, $\chi^{(3)}$ does not show anomaly at T_c for $P = 0.08$ sample. To quantitatively define a cross temperature of the emerging THG signal, we follow the method used in ref. (25) to take the second derivative of $\chi^{(3)}$ concerning temperature as shown in the insets of Fig. 1 (I to L). The onset temperature T_{THG} is determined as the slope change in the temperature dependence of the second derivative. We extract the $T_{\text{THG}} = 270$ K for $P = 0.077$, 260 K for $P = 0.08$, 180 K for $P = 0.10$, 150 K for $P = 0.138$ and 140 K for $P = 0.15$.

We summarize the extracted crossover temperature T_{THG} in Fig. 1O, in which the reported characteristic temperatures of the exotic phases, e.g., fluctuated superconductivity and two-dimensional (2D) charge density wave (CDW), are also displayed as explained in the figure captions. Obviously, the T_{THG} follows the tendency of pseudogap temperature T^* line. It deserves to remark that, within the doping range we measured, the T_{THG} also follows the trend of fluctuated superconductivity, though the T_{THG} deviates from the fluctuated superconductivity temperature T^{onset} notably for the two lowest doping level samples, as illustrated in Fig. 1O.

To provide a solid experimental basis, we perform additional experimental measurements and the results yield further support for the observed correlation. First, it is well accepted that the pseudogap phase is present in the hole-doped side but absent in the electron-doped side in the phase diagram of cuprate. For comparison, we have done similar measurements on an electron-doped cuprate sample $\text{La}_{2-x}\text{Ce}_x\text{CuO}_4$ ($x \sim 0.10$) (LCCO) with $T_c = 24$ K and confirm the absence of THG above its T_c . The THG signals at selective temperatures on LCCO driven by $f = 0.5$ THz and $f = 0.7$ multicycle terahertz pulses are shown in Fig. 1 (M and N). The THG signal disappears abruptly when the temperature is heated up to T_c , similar to the THG response of conventional superconductors (11, 14–16). This comparison highly suggests that the THG signal above T_c is linked to the exotic pseudogap state in hole-doped cuprate superconductors. Second, although the third-order nonlinear process is symmetry allowed in all of the media as long as the driving pulse is strong enough, the observed behavior is different from the contribution of normal quasiparticles without displaying exotic properties. To this purpose, we tried to detect the THG signal driven by strong near-infrared (NIR) pulse with the stimulating electric field about 10 times stronger than the terahertz driving pulse. As shown

in Supplementary Materials, although we can resolve the THG signal with NIR driving, the THG intensity in (S, S) geometry exhibits a characteristic fourfold symmetry expected from the D_{4h} lattice symmetry, likely originating from the intraband acceleration of quasiparticles or interband polarization (33). In contrast, the terahertz THG intensity is essentially isotropic as we shall present below.

With these observations, we suggest that it is the exotic pseudogap state that gives rise to a considerable normal state THG signal in hole-doped cuprate superconductors. However, what kind of order in the pseudogap phase that leads to the THG process remains a mystery. The issue is linked to the origin of the pseudogap for which there have been many different suggestions such as preformed Cooper pairs, 2D or fluctuated CDW order, nematic order, and so on. The implication of our experiments on the interplay between superconductivity and pseudogap will be discussed later.

Having established the connection of the crossing temperature of THG with the pseudogap state, we proceed to examine in detail the THG evolution upon lowering temperature below T_c in an effort to study the possible interaction between the pseudogap and superconducting order parameters. To this end, we examine THG measurement on the nearly optimally doped sample (OP87) with $T_c = 87.4$ K, of which the superconducting transition is sharp, suggesting the homogeneity of the superconductivity phase. As shown in Fig. 1 (H and L), the most pronounced feature of the THG signal driven by 0.5-THz pulse is the presence of a sharp resonant peak below T_c . The peak is also present upon driving by other frequencies. Figure 2A shows the temperature dependence of THG intensity from several different driving frequencies, of which resonance temperature decreases slightly with increasing driving frequency. After taking into account the screening effect, as shown in Fig. 2B, the resonance still survives at all driving frequencies. The presence of resonance when twice the pump pulse frequency matches the superconducting gap frequency ($2\omega = 2\Delta$) and the isotropic THG intensity with respect to the lattice axis are two key ingredients for identifying the Higgs mode dominating THG signal in experiment (11, 13). In cuprates, it is difficult to match the resonance temperature with energy gap value due to the d-wave nature in which the gap amplitude varies from zero at the nodal direction to maximum value along the antinodal direction continuously. Nevertheless, the survived resonance is consistent with the recent theoretical calculation that suggests a broad resonance in cuprate superconductors when ω matches with Δ (34), and suggests that the Higgs mode predominates the THG signal at low temperature. Further support for the assignments comes from the polarization dependence measurement. As mentioned above, the THG response of Higgs mode and Cooper pair breaking or charge density fluctuation process have different polarization dependence. The former is isotropic, while the latter is anisotropic, following the underlying lattice symmetry (13). Figure 2C shows the polarization scan with respect to the lattice axis with (S, S) geometry at the corresponding temperature for resonance. The THG intensity is isotropic within the experimental error. With these observations, we suggest that THG signal in the superconducting state is dominated by the Higgs mode of superconductivity order parameter rather than the Cooper pair breaking. It has been theoretically demonstrated that the presence of disorder/impurity can not only enhance the light-Higgs coupling strength but also modify the polarity of the THG signal contributed by Cooper pair breaking. As disorder increases, the THG response caused by Cooper pair breaking changes from following the underlying lattice

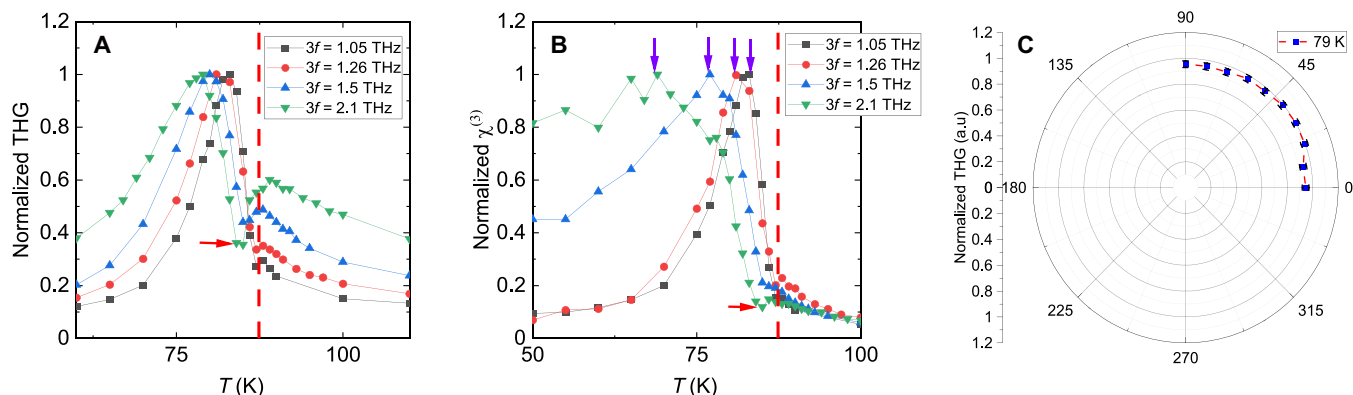


Fig. 2. Temperature and polarization dependence of THG in optimally doped YBCO. (A) Temperature dependence of $I_{3\omega}$ in optimal doped YBCO thin film driven by $\omega = 0.35$ -, 0.42 -, 0.5 -, and 0.7 -THz multicycle pulse. The dashed line indicates the superconductivity transition temperature $T_c = 87.4$ K. The red arrow labels the THG intensity dip at different temperature varying with the frequency of the driven pulse. (B) Temperature dependence of $\chi^{(3)}$ from all driven terahertz pulses plotted with normalized scale. The resonance is still visible after considering the screening effects, suggesting that the Higgs mode is dominating the THG signal. The dip feature still survives after taking account of the screening effect, as labeled by a red arrow. (C) The polarization dependence of $I_{3\omega}$ with (S, S) geometry driven by 0.5 -THz pulse. The sample is rotated with respect to the polarization coplane of fundamental and 3ω photons by a low-temperature piezo rotator. The isotropic response indicates the Higgs mode dominates the THG signal.

symmetry to becoming isotropic (35, 36), which makes it difficult to identify the primary contributor to the THG signal. Recent theoretical analysis has shown that in d-wave cuprate superconductors, the Higgs mode can enhance the Raman response in the symmetric A_{1g} Raman channel (37). However, this conclusion has been heavily debated and challenged by subsequent theoretical work (38). Further research is needed to differentiate between different contributions and to address this issue. It is noteworthy that the resonance behavior vanishes for the $P = 0.138$ doping sample with $T_c = 82$ K. Moreover, the reported THG measurements on different families of optimal hole-doped cuprates, after considering the screening effect, did not show resonance (27). These results may indicate that disorder plays an important role in the detection of Higgs mode in cuprate superconductors. Differentiating between the Higgs and Cooper pair breaking contributions to THG signals is a challenging task. Recent studies have suggested that 2D terahertz spectroscopy, which involves varying both gating time and pump-probe delay time, is an efficient way for distinguishing between the two pathways (39, 40).

Another crucial feature in the temperature-dependent THG signal is that a prominent dip appears near T_c . As shown in Fig. 2A, the THG intensity dip appears at all used driving frequencies and survives after taking account of the screening effect as displayed in Fig. 2B. This observation suggests that the THG in YBCO below T_c cannot be described by assuming that only superconducting condensate contributes to the THG signal. Otherwise, the THG intensity should grow monotonically with decreasing temperature before a resonance appears, as commonly observed in conventional superconductors. To reveal the underlying origin of the dip at the corresponding temperature, we examine the waveforms of the THG signal driven by 0.5 -THz pulse in time domain and corresponding spectra in frequency domain more closely nearby T_c for four different temperatures 90, 86, 85, and 84 K, as shown in Fig. 3. Figure 3 (A to D) shows the time-dependent spectral response obtained by continuous wavelet transformation. At temperature away from T_c , e.g., 90 K above T_c , the THG signal is contributed only from the pseudogap phase, we find a single elliptical structure along the delay time axis

for both fundamental and THG pulses. However, the time-frequency THG intensity mappings in Fig. 3 (B to D) are found to have the obvious dip at 3 ps for 86 K, 4.5 ps for 85 K, and 5.5 ps for 84 K, respectively. Presence of the dip structure coincides with the anomaly in the integrated THG intensity as a function of temperature displayed in Fig. 2A. Figure 3 (E to H) shows the real-time THG waveforms after a digital 1-THz high-pass filter for the four different temperatures. Notably, a beat pattern emerges on the THG oscillations, which is corresponding to the dip in the time-frequency THG intensity mapping. The development of beat indicates the splitting of the THG frequency, which is indeed seen clearly in the FFT spectra, as shown in Fig. 3 (I to L). As can be resolved from the plot, one of the split two peaks is unambiguously pushed down to a lower frequency below 1.5 THz, and the other to a higher frequency above 1.5 THz.

Now, we attempt to identify the nature of the observed beat. The possibility of the Fabry-Perot effect of either the fundamental pulse or THG pulse inside the thin film introducing the experimental feature is ruled out. We record the temperature-dependent waveform of a 1.5 -THz multicycle pulse in linear response regime passing through the thin film. A continued phase shift induced by superconductivity is observed, but no beat pattern is identified around T_c . Then, the beat would indicate that two modes meet at the same energy and result in an energy level repulsion due to their coupling. It is natural to assume that a collective mode is present in the pseudogap phase that produces the THG with the strong multicycle terahertz pulse driving. Upon entering the superconducting state, an additional mode appears at T_c which also generates THG and couples to the mode already developed in the pseudogap phase. We have elaborated above that this new mode developed below T_c should be collective Higgs mode of superconductor. Because both modes are driven by the same fundamental pulse at 0.5 THz, their THG should appear at same frequency. However, because they have different origins, their coupling leads to the energy level splitting.

To resolve the peak splitting more clearly, we analyze the spectral evolution as a function of temperature. Figure 4A shows the normalized THG spectra at several different temperatures. The line shape is seen to change dramatically when the temperature is

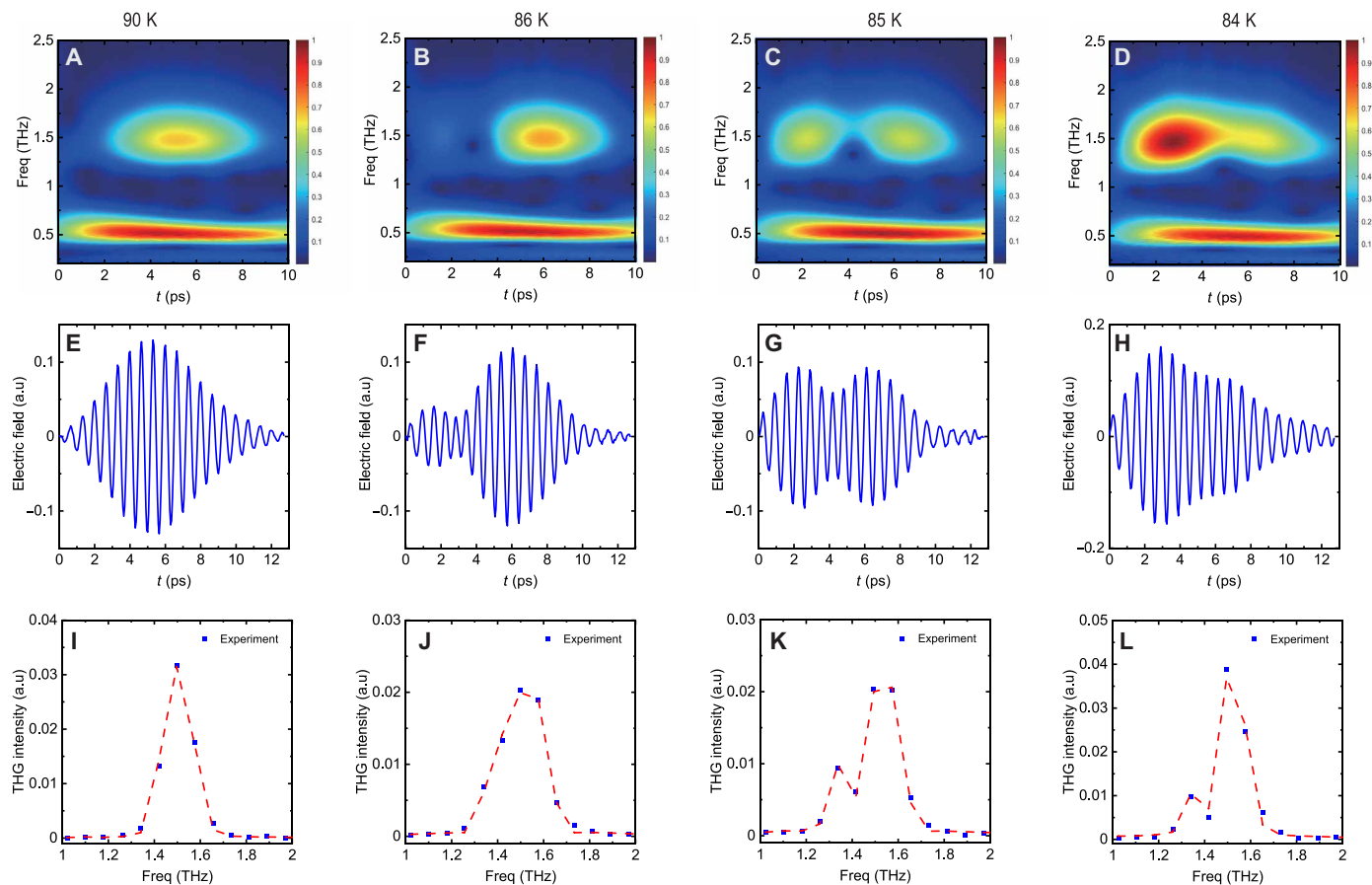


Fig. 3. Time-frequency distribution of THG in optimally doped YBCO. (A to D) THG intensity continuous wavelet transformation (CWT) chromograms in optimal doped YBCO thin film driven by 0.5-THz pulse for (A) 90 K, (B) 86 K, (C) 85 K, and (D) 84 K. The dip at selective delay time in CWT chromograms indicates a destructive interference. (E to H) The real-time waveforms of THG signal after a digital 1-THz high-pass filter. The beating pattern in the waveform is corresponding to the dip in CWT chromogram. (I to L) The THG spectrum for 90, 86, 85, and 84 K after the global FFT. The splitting is caused by the dynamical interaction between Higgs mode and pseudogap collective mode as described in the main text.

decreased, first as a Lorentz profile above T_c , then as a double peak around 85 K, subsequently an asymmetric peak in the intermediate temperature (82 K), and lastly as a symmetric Lorentz peak again below 65 K. Understanding the spectral shape evolution would provide valuable information about the interplay between superconductivity and pseudogap phase. Here, the key is to explain the disappearance of the beat pattern and frequency splitting at temperature far below T_c , where both the superconductivity and the pseudogap/other symmetry broken orders are well established. We speculate two possibilities for the observed phenomena. First, when the temperature drops below the critical temperature T_c , the superconductivity-induced THG signal quickly increases and dominates the waveform profile. To gain insight into the impact this effect would have on the coupling, we simulated the superposition of two Gaussian wavelets with close central frequencies, but one with a significantly higher amplitude than the other. As can be seen in the Supplementary Materials, the beat pattern in the time domain and the spectral splitting in the frequency domain become invisible, with the profile of the waveform in either domain being dominated by the larger amplitude wavelet. This is similar to what is observed

in our optimally doped sample at low temperatures, which explains the difficulty in detecting the coupling structure. In comparison, near T_c , the two THG signals from the normal state and superconductivity have roughly equal amplitudes, thus making the beat pattern and spectral splitting more prominent. This behavior is also seen recently in the NbSe₂ sample (41), where coupling between CDW and superconductivity is clearly defined. Second, the spectral weight may be transferred from the normal state wavelet to the superconducting wavelet at low temperatures, which enhances the intensity of the superconducting wavelet and suppresses the normal state weight. Such spectral weight transfer has been identified in the NbSe₂ sample by Raman and terahertz THG measurements (4, 41) and also been theoretically studied recently (30). Figure 4B displays the polarization dependence of the hybridization, which is isotropic with respect to the lattice axis. Such behavior is not unexpected because both the THG signals arising from Higgs mode and pseudogap phase appear to be isotropic. We emphasize that the above mentioned mode-coupling structures are clearly seen in the nearly optimally doped sample. In the underdoped samples, those features become invisible.

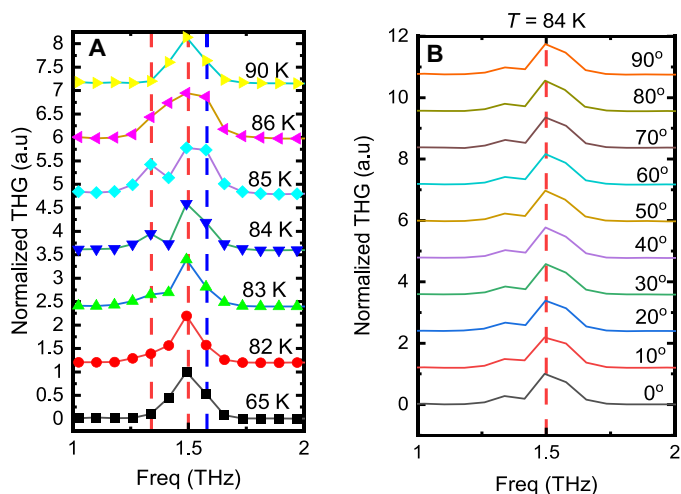


Fig. 4. Temperature dependence of beat structure in optimally doped YBCO. (A) Temperature dependence of the profile of THG spectra. The line shape changes markedly when the temperature is decreased, first as a Lorentz profile above T_c , then as a double peak around 85 K, subsequently an asymmetric peak in the intermediate temperature (82 K), and lastly as a symmetric Lorentz peak again below 65 K. The red and blue dash lines indicate the new peak at the lower-frequency side and spectral enhancement at the high-frequency part, respectively. (B) The isotropic response of the splitting, which is consistent with the isotropic THG response of the Higgs mode and pseudogap phase.

DISCUSSION

Our new experimental results have notable implication for further understanding the interplay between superconductivity and the pseudogap. As is known, the pseudogap phase in hole-doped cuprates is characterized as a depletion of the single-particle spectral weight near the chemical potential below a certain temperature T^* . The origin of the pseudogap is still debated, with two main interpretations being proposed: Either the pseudogap is a precursor to superconductivity, or it arises from a distinctly different order. Within the pseudogap phase, several orders have been identified to exist, such as 2D or fluctuating CDW order, nematic order, and so on. We shall explore the different possibilities in more detail below.

The first possibility is that normal-state THG signal comes from the fluctuated superconductivity or preformed Cooper pairs that lack phase coherence. As we illustrate in Fig. 10, within the doping range we measured, the T_{THG} follows the trend of fluctuated superconductivity temperature T^{onset} , though notable deviation was seen for the two lowest-doping-level samples. Previous terahertz nonlinear Kerr studies on Higgs mode in high- T_c cuprate Bi2212 have also detected signal from preformed Cooper pairs in the normal state (26), in agreement with T^{onset} temperatures determined from equilibrium spectroscopy techniques such as *c*-axis infrared spectroscopy (42, 43). This preformed Cooper pairs picture can explain the observations in the underdoped samples, where no beat pattern near T_c is seen. However, it is very difficult to explain the beat pattern observed in sample close to the optimal doping. This is because, if the pseudogap phase is due to formation of preformed Cooper pairs, once the temperature lowers to T_c , the macroscopic coherence of Cooper pairs will establish the superconductivity state without forming a new superconducting energy gap, leaving only one pathway for generating the THG signal. As a result, no beat pattern in

real-time waveform of THG signal should form. It can be argued that the underdoped samples, due to their higher oxygen deficiency and broader superconducting transitions, may have a lower quality that weakens the coupling effect and renders the feature undetectable. Nevertheless, it is possible that the absence of the beat pattern in the underdoped samples is intrinsic. If this is case, the origin of the THG above T_c for the underdoped samples must be distinct from that of the optimally doped sample. The THG signal in optimally doped sample above T_c may come from, e.g., the CDW order.

The second possibility is that the T_{THG} in the normal state is originated from some symmetry-broken orders being present in the pseudogap phase, such as short-range or fluctuated CDW. Fluctuated CDW is found to exist above T_c ubiquitously in underdoped cuprates (44–47). Earlier nonlinear terahertz response studies on $\text{La}_{2-x}\text{Sr}_x\text{CuO}_4$ at different dopings and magnetic field have indicated the presence of a Higgs-CDW amplitude mode interaction, which is responsible for the Fano interference in THG signals (29). Furthermore, a very recent terahertz-driving study on 2H-NbSe_2 , a system in which superconductivity and CDW coexist and compete, has revealed that both CDW amplitude and Higgs oscillations contribute to the THG signal, leading to a beat pattern in the THG waveforms below T_c (41). Here, we may expect similar CDW contribution to the THG signal in the $\text{YBa}_2\text{Cu}_3\text{O}_{6+x}$ system. However, as seen in Fig. 10, there is a clear discrepancy between the extracted onset temperature of T_{THG} and the T_{CDW} , which has a dome shape as determined by resonant inelastic x-ray spectroscopy (48, 49). The different trends with respect to doping implies that the THG signal in the normal state cannot be solely attributed to the nonlinear response of the CDW mode.

Considering the spectral shape of THG signal and its doping evolution displayed in Fig. 10, it is plausible to suggest that the THG signal below T_{THG} consists of multiple contributions and its predominant contributor may vary with doping in the driving protocol. Close to optimal doping, the fluctuated CDW order is likely to have a greater contribution and its interaction with the Higgs mode developed below T_c is responsible for the beat pattern in the THG waveform in the time domain and splitting in the frequency. At lower doping levels, the fluctuated superconductivity arising from preformed Cooper pairs may dominate the THG signal. Thus, the global phase coherence formed at T_c may not lead to any anomaly of the THG signal or beat pattern in the real-time waveform. To definitively identify the origin of the THG signal of the normal state in cuprates, further systematic investigation on high-quality samples with homogeneous superconductivity is necessary.

Last, we would like to remark that there is also a possibility that the T_{THG} in the normal state is contributed by other orders rather than CDW, for example, nematic order developed within the pseudogap phase. Presence of a nematic order that spontaneously breaks rotation symmetry in YBCO has been evidenced by Nernst effect measurement below T^* (50). Theoretical investigations indicate that the nematic interaction has a strong impact on the short-time dynamics of unconventional superconductors (51). Moreover, recent terahertz Kerr measurements have also identified a clear nematic order contribution in iron-based superconductors (52), while Raman spectroscopy has observed nematic fluctuations in various hole-doped cuprates up to T^* (53). On the basis of these observations, it is possible that nematic order may contribute THG signals up to T^* . However, further theoretical and experimental investigations are necessary to determine the plausibility of this speculation.

On all accounts, the present nonlinear terahertz spectroscopy study with the observation of coupling between collective modes from different sources on sample near optimal doping and its disappearance in samples with lower doping levels offers a fresh perspective for exploration of the nature and interplay between superconductivity and pseudogap in cuprates.

MATERIALS AND METHODS

The $\text{YBa}_2\text{Cu}_3\text{O}_{6+x}$ (YBCO) with different doping levels and the optimally doped $\text{La}_{2-x}\text{Ce}_x\text{CuO}_4$ ($x \sim 0.10$) (LCCO) thin film are prepared by pulsed laser deposition method. T_c is determined from resistivity measurements as shown in the Supplementary Materials. The strong field broadband terahertz pulses are generated via tilted pulse-front scheme using a LiNbO₃ crystal, driven by a Ti:sapphire amplifier generating 100 fs pulses at 800 nm with a pulse energy of 3.2 mJ and a repetition rate of 1 kHz. Narrowband multicycle terahertz pulses are produced using band-pass filters with 20% bandwidth. To suppress the fundamental pulse and enhance the sensitivity of THG response, we use a 3 ω terahertz band-pass filter after the sample. The terahertz radiation is detected by electro-optic sampling with a ZnTe crystal.

Supplementary Materials

This PDF file includes:

Supplementary Text
Figs. S1 to S9
Table S1

REFERENCES AND NOTES

1. B. Keimer, S. A. Kivelson, M. R. Norman, S. Uchida, J. Zaanen, From quantum matter to high-temperature superconductivity in copper oxides. *Nature* **518**, 179–186 (2015).
2. J. A. Sobota, Y. He, Z.-X. Shen, Angle-resolved photoemission studies of quantum materials. *Rev. Mod. Phys.* **93**, 025006 (2021).
3. R. Sooryakumar, M. V. Klein, Raman scattering by superconducting-gap excitations and their coupling to charge-density waves. *Phys. Rev. Lett.* **45**, 660–662 (1980).
4. M.-A. Méasson, Y. Gallais, M. Cazayous, B. Clair, P. Rodière, L. Cario, A. Sacuto, Amplitude higgs mode in the 2H-NbSe₂ superconductor. *Phys. Rev. B* **89**, 060503 (2014).
5. P. W. Anderson, Plasmons, gauge invariance, and mass. *Phys. Rev.* **130**, 439–442 (1963).
6. P. W. Anderson, Random-phase approximation in the theory of superconductivity. *Phys. Rev.* **112**, 1900–1916 (1958).
7. P. B. Littlewood, C. M. Varma, Gauge-invariant theory of the dynamical interaction of charge density waves and superconductivity. *Phys. Rev. Lett.* **47**, 811–814 (1981).
8. C. M. Varma, Higgs Boson in superconductors. *J. Low Temp. Phys.* **126**, 901–909 (2002).
9. J. Hebling, G. Almási, I. Z. Kozma, J. Kuhl, Velocity matching by pulse front tilting for large area thz-pulse generation. *Opt. Express* **10**, 1161–1166 (2002).
10. R. Matsunaga, Y. I. Hamada, K. Makise, Y. Uzawa, H. Terai, Z. Wang, R. Shimano, Higgs amplitude mode in the bcs superconductors $\text{Nb}_{1-x}\text{Ti}_x\text{N}$ induced by terahertz pulse excitation. *Phys. Rev. Lett.* **111**, 057002 (2013).
11. R. Matsunaga, N. Tsuji, H. Fujita, A. Sugioka, K. Makise, Y. Uzawa, H. Terai, Z. Wang, H. Aoki, R. Shimano, Light-induced collective pseudospin precession resonating with higgs mode in a superconductor. *Science* **345**, 1145–1149 (2014).
12. N. Tsuji, H. Aoki, Theory of anderson pseudospin resonance with higgs mode in superconductors. *Phys. Rev. B* **92**, 064508 (2015).
13. R. Matsunaga, N. Tsuji, K. Makise, H. Terai, H. Aoki, R. Shimano, Polarization-resolved terahertz third-harmonic generation in a single-crystal superconductor nbn: Dominance of the higgs mode beyond the bcs approximation. *Phys. Rev. B* **96**, 020505 (2017).
14. F. Giorgianni, T. Cea, C. Vicario, C. P. Hauri, W. K. Witherage, X. Xi, L. Benfatto, Leggett mode controlled by light pulses. *Nat. Phys.* **15**, 341–346 (2019).
15. S. Kovalev, T. Dong, L.-Y. Shi, C. Reinhoffer, T.-Q. Xu, H.-Z. Wang, Y. Wang, Z.-Z. Gan, S. Germanskiy, J.-C. Deinert, I. Ilyakov, P. H. M. van Loosdrecht, D. Wu, N.-L. Wang, J. Demсар, Z. Wang, Band-selective third-harmonic generation in superconducting MgB_2 : Possible evidence for the higgs amplitude mode in the dirty limit. *Phys. Rev. B* **104**, L140505 (2021).
16. Z.-X. Wang, J.-R. Xue, H.-K. Shi, X.-Q. Jia, T. Lin, L.-Y. Shi, T. Dong, F. Wang, N.-L. Wang, Transient higgs oscillations and high-order nonlinear light-higgs coupling in a terahertz wave driven NbN superconductor. *Phys. Rev. B* **105**, L100508 (2022).
17. X. Yang, C. Vaswani, C. Sundahl, M. Mootz, L. Luo, J. H. Kang, I. E. Perakis, C. B. Eom, J. Wang, Lightwave-driven gapless superconductivity and forbidden quantum beats by terahertz symmetry breaking. *Nat. Photonics* **13**, 707–713 (2019).
18. F. Yang, M. W. Wu, Influence of scattering on the optical response of superconductors. *Phys. Rev. B* **102**, 144508 (2020).
19. T. Cea, C. Castellani, L. Benfatto, Nonlinear optical effects and third-harmonic generation in superconductors: Cooper pairs versus higgs mode contribution. *Phys. Rev. B* **93**, 180507 (2016).
20. M. Silaev, Nonlinear electromagnetic response and higgs-mode excitation in BCS superconductors with impurities. *Phys. Rev. B* **99**, 224511 (2019).
21. Y. Murotani, R. Shimano, Nonlinear optical response of collective modes in multiband superconductors assisted by nonmagnetic impurities. *Phys. Rev. B* **99**, 224510 (2019).
22. L. Schwarz, B. Fauseweh, N. Tsuji, N. Cheng, N. Bittner, H. Krull, M. Berciu, G. S. Uhrig, A. P. Schnyder, S. Kaiser, D. Manske, Classification and characterization of nonequilibrium higgs modes in unconventional superconductors. *Nat. Commun.* **11**, 287 (2020).
23. Y. Barlas, C. M. Varma, Amplitude or higgs modes in d -wave superconductors. *Phys. Rev. B* **87**, 054503 (2013).
24. Z. M. Raines, V. G. Stanev, V. M. Galitski, Hybridization of higgs modes in a bond-density-wave state in cuprates. *Phys. Rev. B* **92**, 184511 (2015).
25. K. Katsumi, N. Tsuji, Y. I. Hamada, R. Matsunaga, J. Schneeloch, R. D. Zhong, G. D. Gu, H. Aoki, Y. Gallais, R. Shimano, Higgs mode in the d -wave superconductor $\text{Bi}_2\text{Sr}_2\text{CaCu}_2\text{O}_{8+x}$ driven by an intense terahertz pulse. *Phys. Rev. Lett.* **120**, 117001 (2018).
26. K. Katsumi, Z. Z. Li, H. Raffy, Y. Gallais, R. Shimano, Superconducting fluctuations probed by the higgs mode in $\text{Bi}_2\text{Sr}_2\text{CaCu}_2\text{O}_{8+x}$ thin films. *Phys. Rev. B* **102**, 054510 (2020).
27. H. Chu, M. J. Kim, K. Katsumi, S. Kovalev, R. D. Dawson, L. Schwarz, N. Yoshikawa, G. Kim, D. Putzky, Z. Z. Li, H. Raffy, S. Germanskiy, J. C. Deinert, N. Awari, I. Ilyakov, B. Green, M. Chen, M. Bawatna, G. Cristiani, G. Logvenov, Y. Gallais, A. V. Boris, B. Keimer, A. P. Schnyder, D. Manske, M. Gensch, Z. Wang, R. Shimano, S. Kaiser, Phase-resolved higgs response in superconducting cuprates. *Nat. Commun.* **11**, 1793 (2020).
28. R. Shimano, N. Tsuji, Higgs mode in superconductors. *Annu. Rev. Condens. Matter Phys.* **11**, 103–124 (2020).
29. H. Chu, S. Kovalev, Z. X. Wang, L. Schwarz, T. Dong, L. Feng, R. Haenel, M.-J. Kim, P. Shabestari, L. P. Hoang, K. Honasoge, R. D. Dawson, D. Putzky, G. Kim, M. Puviani, M. Chen, N. Awari, A. N. Ponomaryov, I. Ilyakov, M. Bluschke, F. Boschini, M. Zonno, S. Zhdanovich, M. Na, G. Cristiani, G. Logvenov, D. J. Jones, A. Damascelli, M. Minola, B. Keimer, D. Manske, N. Wang, J.-C. Deinert, S. Kaiser, Fano interference between collective modes in cuprate high- T_c superconductors. *Nat. Commun.* **14**, 1343 (2023).
30. L. Schwarz, R. Haenel, D. Manske, Phase signatures in the third-harmonic response of higgs and coexisting modes in superconductors. *Phys. Rev. B* **104**, 174508 (2021).
31. C. Vaswani, J. H. Kang, M. Mootz, L. Luo, X. Yang, C. Sundahl, D. Cheng, C. Huang, R. H. J. Kim, Z. Liu, Y. G. Collantes, E. E. Hellstrom, I. E. Perakis, C. B. Eom, J. Wang, Light quantum control of persisting higgs modes in iron-based superconductors. *Nat. Commun.* **12**, 258 (2021).
32. K. Isoyama, N. Yoshikawa, K. Katsumi, J. Wong, N. Shikama, Y. Sakishita, F. Nabeshima, A. Maeda, R. Shimano, Light-induced enhancement of superconductivity in iron-based superconductor $\text{FeSe}_{0.5}\text{Te}_{0.5}$. *Commun. Phys.* **4**, 160 (2021).
33. S. Ghimire, D. A. Reis, High-harmonic generation from solids. *Nat. Phys.* **15**, 10–16 (2019).
34. L. Schwarz, D. Manske, Theory of driven higgs oscillations and third-harmonic generation in unconventional superconductors. *Phys. Rev. B* **101**, 184519 (2020).
35. M. Udina, J. Fiore, T. Cea, C. Castellani, G. Seibold, L. Benfatto, THz non-linear optical response in cuprates: Predominance of the BCS response over the Higgs mode. *Faraday Discuss.* **237**, 168–185 (2022).
36. G. Seibold, M. Udina, C. Castellani, L. Benfatto, Third harmonic generation from collective modes in disordered superconductors. *Phys. Rev. B* **103**, 014512 (2021).
37. M. Puviani, A. Baum, S. Ono, Y. Ando, R. Hackl, D. Manske, Calculation of an enhanced A_{1g} symmetry mode induced by higgs oscillations in the raman spectrum of high-temperature cuprate superconductors. *Phys. Rev. Lett.* **127**, 197001 (2021).
38. L. Benfatto, C. Castellani, T. Cea, Comment on “calculation of an enhanced A_{1g} symmetry mode induced by higgs oscillations in the raman spectrum of high-temperature cuprate superconductors”. *Phys. Rev. Lett.* **129**, 199701 (2022).
39. L. Luo, M. Mootz, J. H. Kang, C. Huang, K. Eom, J. W. Lee, C. Vaswani, Y. G. Collantes, E. E. Hellstrom, I. E. Perakis, C. B. Eom, J. Wang, Quantum coherence tomography of light-controlled superconductivity. *Nat. Phys.* **19**, 201–209 (2023).
40. M.-J. Kim, S. Kovalev, M. Udina, R. Haenel, G. Kim, M. Puviani, G. Cristiani, I. Ilyakov, T. V. A. G. de Oliveira, A. Ponomaryov, J.-C. Deinert, G. Logvenov, B. Keimer, D. Manske, L. Benfatto, S. Kaiser, Tracing the dynamics of superconducting order via transient third harmonic generation. *arXiv:2303.03288 [cond-mat.supr-con]* (6 March 2023).
41. L. Feng, J. Cao, T. Priessnitz, Y. Dai, T. D. Oliveira, J. Yuan, G. Kim, G. Cristiani, G. Logvenov, B. Keimer, D. Wu, Y. Huang, J.-C. Deinert, S. Kovalev, T. Dong, N. Wang, S. Kaiser, H. Chu,

- Dynamical interplay between superconductivity and charge-density-wave: A nonlinear terahertz study of coherently-driven 2H-NbSe₂ and La_{2-x}Sr_xCuO₄. arXiv:2211.10947 [cond-mat.supr-con] (20 November 2022).
42. A. Dubroka, M. Rössle, K. W. Kim, V. K. Malik, D. Munzar, D. N. Basov, A. A. Schafgans, S. J. Moon, C. T. Lin, D. Haug, V. Hinkov, B. Keimer, T. Wolf, J. G. Storey, J. L. Tallon, C. Bernhard, Evidence of a precursor superconducting phase at temperatures as high as 180 K in RBa₂Cu₃O_{7-δ} (R = Y, Gd, Eu) superconducting crystals from infrared spectroscopy. *Phys. Rev. Lett.* **106**, 047006 (2011).
 43. E. Uykur, K. Tanaka, T. Masui, S. Miyasaka, S. Tajima, Persistence of the superconducting condensate far above the critical temperature of YBa₂(Cu, Zn)₃O_y revealed by *c*-axis optical conductivity measurements for several Zn concentrations and carrier doping levels. *Phys. Rev. Lett.* **112**, 127003 (2014).
 44. R. Arpaia, S. Caprara, R. Fumagalli, G. De Vecchi, Y. Y. Peng, E. Andersson, D. Betto, G. M. De Luca, N. B. Brookes, F. Lombardi, M. Salluzzo, L. Braicovich, C. Di Castro, M. Grilli, G. Ghiringhelli, Dynamical charge density fluctuations pervading the phase diagram of a Cu-based high-*T_c* superconductor. *Science* **365**, 906–910 (2019).
 45. B. Yu, W. Tabis, I. Bialo, F. Yakhou, N. B. Brookes, Z. Anderson, Y. Tang, G. Yu, M. Greven, Unusual dynamic charge correlations in simple-tetragonal HgBa₂CuO_{4+δ}. *Phys. Rev. X* **10**, 021059 (2020).
 46. L. Wang, B. Yu, R. Jing, X. Luo, J. Zeng, J. Li, I. Bialo, M. Bluschke, Y. Tang, J. Freyermuth, G. Yu, R. Sutarto, F. He, E. Weschke, W. Tabis, M. Greven, Y. Li, Doping-dependent phonon anomaly and charge-order phenomena in the HgBa₂CaCu₂O_{4+δ} and HgBa₂CaCu₂O_{6+δ} superconductors. *Phys. Rev. B* **101**, 220509 (2020).
 47. R. Arpaia, G. Ghiringhelli, Charge order at high temperature in cuprate superconductors. *J. Physical Soc. Jpn* **90**, 111005 (2021).
 48. G. Ghiringhelli, M. Le Tacon, M. Minola, S. Blanco-Canosa, C. Mazzoli, N. B. Brookes, G. M. De Luca, A. Frano, D. G. Hawthorn, F. He, T. Loew, M. M. Sala, D. C. Peets, M. Salluzzo, E. Schierle, R. Sutarto, G. A. Sawatzky, E. Weschke, B. Keimer, L. Braicovich, Long-range incommensurate charge fluctuations in (Y, Nd) Ba₂Cu₃O_{6+x}. *Science* **337**, 821–825 (2012).
 49. S. Blanco-Canosa, A. Frano, E. Schierle, J. Porras, T. Loew, M. Minola, M. Bluschke, E. Weschke, B. Keimer, M. Le Tacon, Resonant x-ray scattering study of charge-density wave correlations in YBa₂Cu₃O_{6+x}. *Phys. Rev. B* **90**, 054513 (2014).
 50. R. Daou, J. Chang, D. LeBoeuf, O. Cyr-Choinière, F. Laliberte, N. Doiron-Leyraud, B. J. Ramshaw, R. Liang, D. A. Bonn, W. N. Hardy, L. Taillefer, Broken rotational symmetry in the pseudogap phase of a high-*t_c* superconductor. *Nature* **463**, 519–522 (2010).
 51. M. A. Müller, P. A. Volkov, I. Paul, I. M. Eremin, Interplay between nematicity and *b_{1g}*-*b_{2g}* modes in the short-time dynamics of unconventional superconductors. *Phys. Rev. B* **103**, 024519 (2021).
 52. R. Grasset, K. Katsumi, P. Massat, H.-H. Wen, X.-H. Chen, Y. Gallais, R. Shimano, Terahertz pulse-driven collective mode in the nematic superconducting state of Ba_{1-x}K_xFe₂As₂. *npj Quantum Mater.* **7**, 4 (2022).
 53. N. Auvray, B. Loret, S. Benhabib, M. Cazayous, R. D. Zhong, J. Schneeloch, G. D. Gu, A. Forget, D. Colson, I. Paul, A. Sacuto, Y. Gallais, Nematic fluctuations in the cuprate superconductor Bi₂Sr₂CaCu₂O_{8+δ}. *Nat. Commun.* **10**, 5209 (2019).
 54. B. Fauqué, Y. Sidis, V. Hinkov, S. Pailhès, C. T. Lin, X. Chaud, P. Bourges, Magnetic order in the pseudogap phase of high-*T_c* superconductors. *Phys. Rev. Lett.* **96**, 197001 (2006).
 55. J. Xia, E. Schemm, G. Deutscher, S. A. Kivelson, D. A. Bonn, W. N. Hardy, R. Liang, W. Siemons, G. Koster, M. M. Fejer, A. Kapitulnik, Polar Kerr-effect measurements of the high-temperature YBa₂Cu₃O_{6+x} superconductor: Evidence for broken symmetry near the pseudogap temperature. *Phys. Rev. Lett.* **100**, 127002 (2008).
 56. R. Liang, D. A. Bonn, W. N. Hardy, Evaluation of CuO₂ plane hole doping in YBa₂Cu₃O_{6+x} single crystals. *Phys. Rev. B* **73**, 180505 (2006).
- Acknowledgments:** We gratefully acknowledge H. Chu, Y. Wan, and Q. Zhang for illuminating discussions. The linear terahertz spectroscopy on optimal doped YBCO sample was carried out at the Synergetic Extreme Condition User Facility (SECUF). **Funding:** This work was supported by the National Science Foundation of China (nos. 11888101, 11974414, and 12134018) and the National Key Research and Development Program of China (2021YFA1400200, 2022YFA1403900, and 2022YFA1603903). **Author contributions:** T.D. and N.W. conceived the project. J.Y., L.S., and Z.W. performed the terahertz THG measurements of the cuprate thin films with help from S.X., Q.W., S.Z., Q.L., T.H., X.Z., R.L., B.L. and D.W. T.X., Y.W., and Z.G. prepared and characterized the different doping YBCO thin films. F.C., Z.L., Xu Wang, and K.J. prepared and characterized the optimal doped YBCO and LCCO thin films. L.Y. measured the THG response on optimal doped YBCO thin films at room temperature with 1300-nm pulse. The linear terahertz spectroscopy on optimal doped YBCO sample was carried out at the Synergetic Extreme Condition User Facility (SECUF) by Xinbo Wang and J.L. J.Y., T.D., and N.W. interpreted the data and wrote this paper, with inputs from all the authors. **Competing interests:** The authors declare that they have no competing interests. **Data and materials availability:** All data needed to evaluate the conclusions in the paper are present in the paper and/or the Supplementary Materials.
- Submitted 2 February 2023
Accepted 10 January 2024
Published 9 February 2024
10.1126/sciadv.adg9211